Supplemental File S1, Theory

In this supplementary note, we develop a theoretical model for the mechanics of the emergence of an apical epithelial surface in the multi-ciliated cells (MCCs) of the *Xenopus laevis* epidermis. In particular, and guided by the experimental results described in the main text, we concentrate on the role of the forces exerted by the actomyosin cytoskeleton. This is in agreement with many previous studies that underlie the crucial contribution of actomyosin to cellular mechanics in general, both *in vivo* and *in vivo* (Salbreux et al. 2001, Heisenberg et al, 2013, Sedzinski et al, 2011, Marcy et al. 2004, Demoulin et al. 2014, Maitre et al. 2012, Bertet et al. 2004, Marinari et al. 2012). Even though the mechanics underlying the extrusion of cell from a monolayer are starting to be better understood, involving an active constriction of the apical actomyosin ring (Marinari et al. 2012, Wu et al, 2015), very little is known of the mechanics of cell intercalation within a monolayer, i.e. the emergence of a mature apical surface. Therefore, our strategy is to consider all possible force contribution to the emergence, examine what would be their effect of cell shape and tissue stress, and test each prediction successively. The model we describe here is two-dimensional, and applies to the apical surfaces of the intercalating cells and their neighbours. The reasons for this choice, as well as extension to three-dimensions, are discussed in the last paragraph of this note.

At the apical surface of most epithelial cells, actin is segregated into two pools : a junctional pool at the cell-cell boundaries, forming rings which are connected from cell to cell by the adherens junction complex (Tsukita et al, 1992), and a medial pool in the center of the apical surface (Rauzi et al, 2010). At this stage of embryo development, this medial pool is uniform and does not display additional segregation, into specialized cilia structures for instance.

As junctional actomyosin is condensed into a thin, well-defined layer cortical layer, it is reasonable to model its contribution as a line tension, with the value of this tension increasing with actin and myosin concentration. This leads to a strong analogy between the physics of epithelial packing and of soap films, as both tend to minimise their perimeter. Both can be described by vertex models (Graner et al, 1992, Farhadifar et al, 2007), which assume junctions to be straight lines, or cellular Potts models (Fletcher et al, 2014), which relax this assumption. Recently, the same sort of description was extended to three-dimensional settings (Hannezo et al, 2014).

In two-dimensional vertex-type models, an additional contribution must be added for the stability of the epithelium, dependent on the apical area. In principle, it can be either positive (representing a pressure exerted by the apical area) or negative (representing a tension exerted by the apical area).

In the following text, instead of concentrating on large-scale properties of cell packing, which was the goal of many vertex-type simulations (Graner et al, 1992, Fletcher et al, 2014, Mao et al, 2013), we zoom in on a single intercalating cell, and write the balance of force on its apical surface, taking into account both junctional mechanics (line terms) and area mechanics (surface terms). In contrast with vertex models, we allow the intercalating cell to have any shape. Importantly, one should note that the detailed shape of the cell contains much information of the forces in play, and in particular on the ratio of junctional vs surface forces, as we detail below.

From a theoretical perspective, there are two broad classes of mechanisms : cell-autonomous, where the MCCs drives the apical expansion (pushing force) and the neighbours resist it, and non-cell autonomous, where the neighbours drive the apical expansion (pulling force, either from the perpendicular junctions or the neighbour medial pool) and the MCCs resist it.

In order to know the sign of each contribution, laser-dissection experiments are extremely useful. As described in the main text, junction dissection always resulted in retraction, meaning that junctions from the intercalating and neighborings cells are under tension. Laser dissection in the medial pool of neighborings cells lead to a discernable recoil, but crucially, ablating either the perpendicular junctions or the medial actin pool of the neighbouring cells during MCC intercalation did not lead to any MCC collapse, which would be the case if neighbour tension was driving the process. This leads us to neglect neighbour area tension in

the following, and to assume that at least the first phase of apical surface emergence is cell-autonomous, an hypothesis which we subsequently check experimentally.

1 Force balance on the intercalating cell

We call $r(\theta, t)$ the radius of the expanding apical domain of the intercalating MCC, as a function of the polar angle θ and time t. We write force balance on the intercalating MCC, taking into account all possible contributions (see Theory Figure S1)

$$\eta \partial_t r = \delta P - Er - \gamma \mathcal{C} + \sum_{i=1}^{N} \Lambda_i \delta(\theta - \theta_i) \tag{1}$$

where

$$\mathcal{C}(\theta, t) = \frac{r^2 + (\partial_\theta r)^2 - r\partial_{\theta\theta} r}{(r^2 + (\partial_\theta r)^2)^{3/2}}$$

is the local curvature of the MCC apical junction, and η the viscosity of the cortex. The possible contributions to force balance are :

- a pressure δP exerted by the MCC on its surroundings, helping expansion.
- cortical line tensions Λ_i from the perpendicular junctions of the neighbours, helping expansion
- a resistance from the neighbours to expansion, modelled as a linear spring of stiffness E.
- a cortical line tension γ from the MCC, resisting expansion
- an effective viscosity η which describes the viscous forces associated with apical expansion.

2 Expansion and resisting force

Let's start with a few limits at steady state ($t \to \infty$).

- If the pressure forces are very large compared to the junctional forces (δP, $Er \gg \Lambda/r$, Λ/r), then we expect the cell to be round, and reach the radius $r_0 = \frac{\delta P}{E}$.
- In the converse case of dominant junctional tension, we expect the cell edges to be straight and make sharp angles. We can simplify the problem to a balance of forces at the vertices, and assume that three perpendicular junctions are pulling on the expanding apical domain. We note a the length of perpendicular junctions and r the side of the expanding apical domain (see Theory Figure S2).

  The energy of the system is

  $$\mathcal{E} = -3\gamma r + 3\Lambda a$$

  Assuming that the outer vertex of perpendicular junction is fixed, and noting a_0 maximal length of perpendicular junction (when $r = 0$) leads a geometrical relationship between a and r : $r = \sqrt{3}(a_0 - a)$.

  From energy minimization, we see that the system has two energy minima:

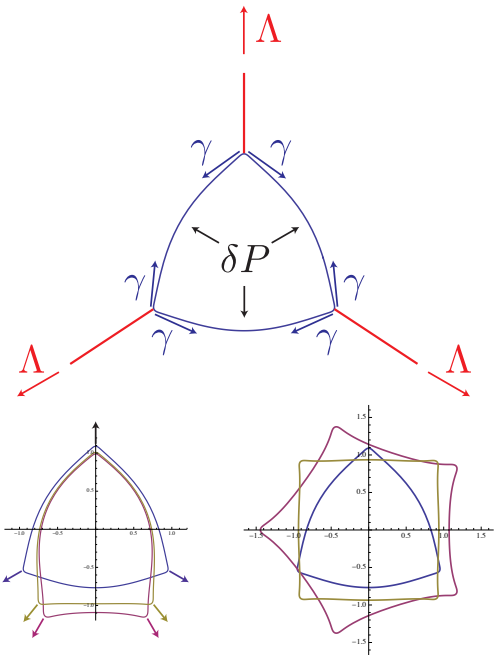

Theory Figure S 1: Top panel : Schematics of our model of force balance for an MCC. Bottom panel : Steady shape of cells under a combination of internal pressure and pulling forces from perpendicular junctions. Left : Varying the position of junctions changes the shape and convexity of the cell. Right : Increasing the number of pulling junctions increases the average cell area, and changes the sign of the curvature of the junctions.

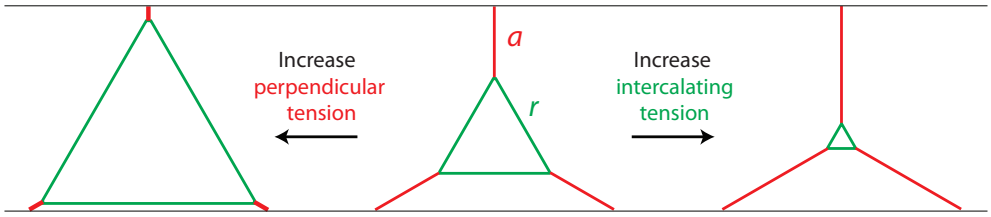

Theory Figure S 2: Schematics of an apical expansion driven by perpendicular cell tensions.

- if $\Lambda < \sqrt{3}\gamma$, the cell collapse entirely ($r = 0$).
- if $\Lambda > \sqrt{3}\gamma$, the cell expands and the perpendicular junction vanishes ($a = 0$).

Another way to see that is that the geometry of the cell makes it so that each vertex must have a 60 degree angle, a condition which can only be respected if $\Lambda = \sqrt{3}\gamma$ exactly. Therefore, an intermediary minimum with perpendicular junctions of finite size requires the existence of pressure and resistance from the neighbors.

- In the case of $\Lambda = 0$ and $E = 0$ (no perpendicular junction, no external rigidity), there is a critical nucleation radius $r_n = \frac{\gamma}{\delta P}$ that the cell has a pass in order to be able to grow, in order not to be

crushed by its tension γ. Cells having a radius lower than r_n would collapse, whereas cells having a radius higher than r_n would grow indefinitely. Obviously, this is unphysical, and the external rigidity prevents this.

- In the case $\Lambda = 0$ and with an external rigidity E, cells remain round, and Eq. (1) simplifies at steady state to

$$\delta P = Er + \frac{\gamma}{r}$$

, which yields a radius of

$$r = \frac{\delta P + \sqrt{\delta P^2 - 4E\gamma}}{2E}$$

This means that an equilibrium can only exist above a critical pressure, i.e. $\delta P > \delta P_c = 2\sqrt{E\gamma}$, which increases with increasing rigidity and tension, as expected. The minimal radius observable in that case is $r_{min} = \frac{\delta P}{2E}$.

- If all forces are present, then one expects to move continuously between the difference regimes, and numerical integration are necessary, as detailed below. One should note that Eq. (1) has a simple analytical steady state solution in the limit $r \to \infty$, i.e. in a planar geometry. One can rewrite force balance on a deflection $r = \epsilon$ due to a point force Λ in $x = 0$

$$0 = -E\epsilon + \gamma\Delta\epsilon - \Lambda\delta(x)$$

which has the solution

$$\epsilon(x) = \frac{\Lambda}{2El}\left(e^{x/l}(1 - \mathcal{H}(x)) + e^{-x/l}\right)$$

where we defined $l = \sqrt{\frac{\gamma}{E}}$, which is the length on which the deformation imposed by the perpendicular junction decays. $\mathcal{H}(x)$ is the Heaviside step function. The above expression can be readily generalised to an arbitrary number of perpendicular junctions $\Lambda_i\delta(x - x_i)$

We also expect the position and number of perpendicular junctions to play a role in the later refining of MCCs' shape. Theory Figure S1 displays two examples of this. Taking perpendicular junctions closer to each others favour a local inversion of curvature, arising from angle equilibration at the vertices. Increasing the number of perpendicular junctions (although maintaining their regular spacing) from 3 to 5 causes larger cells, as well as an inversion of curvature.

3 Measurement of angularity

In the wild type, it is rather apparent that there is three phases of apical expansion: cells remaining at a very small radius, fast expansion phase with a circular cell, plateauing of the cell radius while transitioning from round to triangular shapes. In order to quantify this in an automated and objectif manner, we extract from the data the profiles $r(\theta, t)$ at successive time points, compute the curvature $\mathcal{C}(\theta_i, t)$ for every degree $\theta_i \in [0, 360]$.

We then calculate the time evolution of the mean curvature:

$$\mu_1(t) = \frac{\sum_{\theta_i=0}^{360} \mathcal{C}(\theta_i, t)}{360}$$

the variance:

$$\sigma(t) = \sqrt{\frac{\sum_{\theta_i=0}^{360} (\mathcal{C}(\theta_i, t) - \mu_1)^2}{360}}$$

the fourth moment:

$$\mu_4(t) = \frac{\sum_{\theta_i=0}^{360} (\mathcal{C}(\theta_i, t) - \mu_1)^4}{360}$$

and finally the excess kurtosis:

$$K(t) = \frac{\mu_4}{\sigma^4} - 3$$

The advantage of the excess kurtosis as defined above is that it is equal to zero either for a cell which is perfectly circular ($r = r_0$), or for $r(\theta_i)$ being a normal distribution. This means that random fluctuations in the cell radius (either due to biological noise or segmentation inaccuracies) do not show up in this measurement.

The excess kurtosis is routinely used to quantify how much a distribution has heavy tails, i.e. extreme values, compared to the normal distribution. Therefore, we expect it to be zero for circular cells, but to become very large for angular cells (i.e. which have very high values for curvature at the perpendicular junctions, and very small values otherwise). For this reason, we term it "angularity parameter" in the main text.

Obviously, one could have used other measures for the angularity. The variance of the distribution could be used theoretically, but our analysis showed that it is more sensitive to noise (as we note above), but also that cells sometimes grow as ellipsoids instead of circles. In that case, the variance σ increases, whereas the excess kurtosis K is largely unaffected. As these were not angular cells per se, it demonstrates the superiority of excess kurtosis as a reporter of angularity.

4 Numerical integration of Eq. 1

Let us go back to Eq. 1. The data from the main text, in particular the laser ablation experiments, as well as the rapid cellular collapse with FMN1 KD and SMIFH2 strongly suggests that the viscoelastic time scale of the problem is small $\tau_v = \frac{\eta}{\delta P} \approx 10^1 - 10^2 s$, in line with previous estimates (Salbreux et al, 2012). This means that the slow dynamics of apical expansion (on the timescale of hours) is driven by the slow increase of pressure forces, instead of viscous dissipation. We can then neglect $\eta \to 0$ and assume a sigmoidal increase for the pressure

$$\delta P = \frac{\delta P_0}{1 + e^{-\frac{t - t_0}{\tau_p}}}$$

The time at which pressure increase t_0 is arbitrary and unimportant to this problem, so we set it to zero without loss of generality. We extract the mean expansion time $\tau_p = 20min$ from the data in Fig. 1D of the main text.

We rescale the radius r by $r_0 = \delta P_0 / E$, the time by τ_p and the tensions by $\delta P_0 r_0$. The system of equation then simplifies to

$$\begin{cases} 0 = \delta P - r + \gamma \Delta_\theta r - \Lambda \sum_{i=1}^{N} \delta(\theta - \theta_i) \\ \delta P = \frac{1}{1+e^{-t}} \end{cases} \tag{2}$$

which only contains two ajustable rescaled parameters Λ and γ.

Nevertheless, our data shows unambiguously that both of these tensions change rather significantly in time, and that this time evolution is essential to understand the shape and expansion profile of MCCs. As

we show in the main text, the angularity of the wild type cells is very low during the main phase of the apical expansion, and peaks to high values above a radius threshold of around $r \approx 8 - 9\mu$m.

The simplest, first order theory is then to assume that the tensions are actively regulated by the apical radius of the MCCs:

$$\tau \frac{d\gamma}{dt} = \gamma_0 r - \gamma \tag{3}$$

where γ_0 is a target tension for the largest rescaled radii ($r \approx 1$) and τ a delay time between radius change and tension ajustement.

One can write a similar equation for Λ. Nevertheless, to avoid overfitting the data, we made the assumptions that the two tensions are proportional. We this note $\Lambda = \alpha\gamma$, α being a positive coefficient.

We performed our numerical integrations both by using the dedicated functions in Mathematica, and by using the solver Xmds (Collecut et al, 2011), and got identical results. In order to simulate the perpendicular junctions, we approach the delta functions of Eq. (1) by very peaked gaussian distributions centered around the same values, and with very small variance $\sigma = \frac{2\pi}{500}$. We verified that changing this value, keeping the total force constant, did not modify the results.

To get the fit from the cell seen in the main text, we fit both the time evolution of the angularity of the cell as well as of the apical radius. For the cell shown in the main text, we extracted the parameters $\gamma_0 = 0.45$ and $\alpha = 1.4$, as well as $\tau = 4.5$, which reproduce well also the shape changes undergone by the apical surface.

We also plot the final shape of cells for different values of these tensions in order to explore further the phase diagram (Theory Figure S4):

- increasing both rescaled tensions, ($\gamma_0 = 0.5$, and keeping $\alpha = 1.4$) yields triangular cells.
- decreasing both rescaled tensions ($\gamma_0 = 0.05$, and keeping $\alpha = 1.4$) yields large and very round cells.
- decreasing the perpendicular junction tensions and increasing the cortical tension ($\gamma_0 = 0.6$, and keeping $\alpha = 0.5$) yields very round cells, which are much smaller than wild-type.
- increasing the perpendicular junction tensions and decreasing the cortical tension ($\gamma_0 = 0.2$, and keeping $\alpha = 1.6$) yields large cells which are star-shaped.

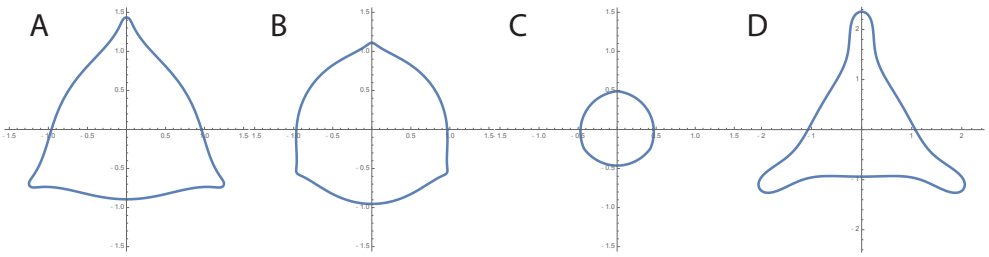

Theory Figure S 3: Numerical integration of cell shapes, in different regions of the phase diagram: low tensions (A), high tensions (B), high cortical tension and low perpendicular tension (C) and low cortical tension/high perpendicular tension (D). The values for the parameters and details on the numerical integration are given in the main text.

In order to highlight the importance of the delay time τ, we forget about Eq. 3, and use the following toy simulation (Theory Figure S4). We keep the values of tensions to zero until a time t_c, and then increase them

abruptly to $\gamma_0 = 0.5$, $\alpha = 1$. For high value of t_c (top panel), the cell had time to get above the nucleation threshold, and apical expansion occurs smoothly. For low values of t_c (bottom panel), the increases in cell tension occurs two early, and the nucleation radius becomes larger than the cell radius, causing collapse.

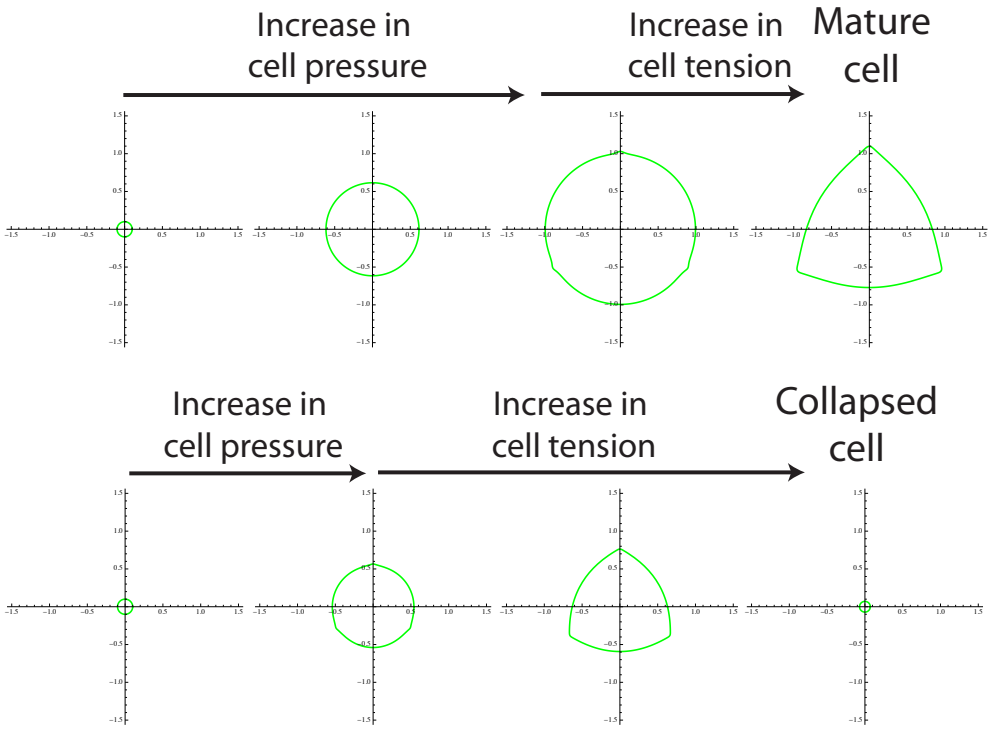

Theory Figure S 4: Dynamics of cellular apical expansion. Top panel : initially, the tensions are negligible, and the cells grow spherically. As the final radius is reached, the tensions become significant, leading to a refinement of shapes and angles, towards a mature epithelium. Bottom panel : if the tensions increase too early, or if the pressure is too small, the cells pass below the nucleation threshold, and collapse.

Similar collapse and oscillatory behaviours occurs when changing γ_0 and δP. For the phase diagram of Fig. 4 in the main text, we therefore fixed $\tau = 5$ and explored 100 simulations for various values of γ_0 and δP, to extract the transition lines between phases. We define a cell as oscillatory if its maximal radius is superior by 5% to its final radius.

5 Three-dimensional aspect of cell apical expansion

The main hypothesis that we explore in the main text is that an effective 2D pressure drives apical expansion. In principle, one could also assume that mechanical forces in 3D, i.e. the lateral tensions, play a role. From a theoretical perspective, it has been shown that the basolateral tensions can contribute to this effective 2D pressure through three-dimensional incompressibility (Hannezo et al, 2014). Intuitively, if lateral tension increases in the MCC, shortening the lateral sides, this provides a force outward driving expansion, qualitatively similar to our 2D pressure.

This bears a strong ressemblance to the physics of cell-doublets (Maitre et al, 2012), as well as cytokinesis (Turlier et al. 2014). In the latter case, Turlier et al. have developed an elegant scaling model where the ratio of cytokinetic ring tension (apical tension in our case) and pole tension (lateral tension in our case) determines the advancement of cytokinesis.

Similarly here, one can define $\kappa = \frac{\gamma}{\Gamma_l R_0}$, where Γ_l is the lateral tension, γ the apical line tension as before, and R_0 the initial 3D radius of the MCC.

One can deduce from energy minimisation consideration, that assuming incompressibility, MCC apical expansion can only proceed if κ goes below a critical threshold $\kappa < \kappa_c \approx 0.4$, i.e. if the lateral tension goes above a critical tension

$$\Gamma_l > \frac{\gamma}{\kappa_c R_0}$$

In our case, the volume of the MCC does increase, which would modify the threshold in the above criteria, but the same physics holds.

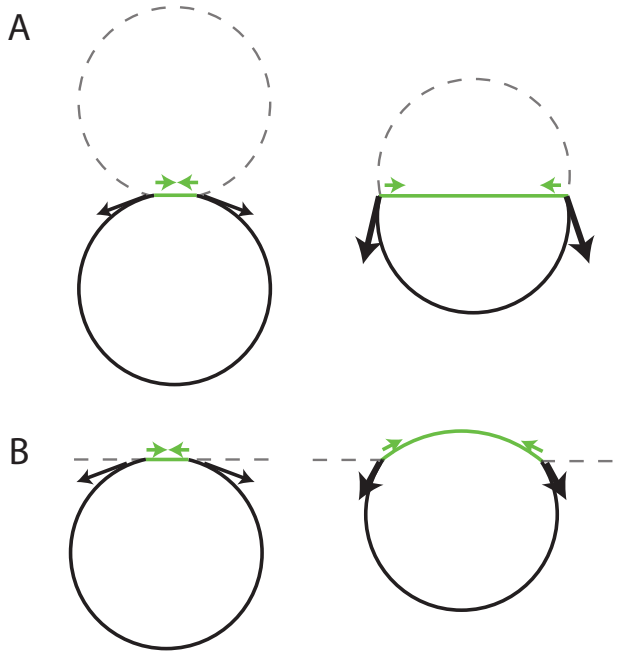

Theory Figure S 5: Schematics of apical expansion in 3D.

Nevertheless, our data provides four arguments against such a mechanism :

- the cortical tension γ actually increases during most of the apical expansion, as shown in our laser ablation experiments (barring a decrease in very early stages). This goes in the opposite direction and tends to diminish apical area.
- actin and myosin display very weak localisation on the basolateral side on the cell, and do not seem to increase as apical expansion proceeds, opposite to what would be expected if Γ_l increased.
- As in cell-doublet systems (Maitre et al. 2012), such a force balance creates sharp and well-defined angles between the apical and lateral sides (Theory Figure S5A), which is again not the case in our 3D reconstructions.

- Last, but not least, in this system, the main difference with cell doublets is that there is not a second cell capable of balancing vertical forces applied by the lateral membrane. Therefore, to balance such forces, the apical surface would have to become curved upwards (see schematics on Theory Figure S5B), which is again not the case.

Supplemental references

Bertet, C., Sulak, L., and Lecuit, T. (2004). Myosin-dependent junction remodelling controls planar cell intercalation and axis elongation. Nature, 429(6992), 667-671.

Collecutt, G., and Drummond, P. D. (2001). xmds: eXtensible multi-dimensional simulator. Computer physics communications, 142(1), 219-223.

Demoulin, D., Carlier, M. F., Bibette, J., and Baudry, J. (2014). Power transduction of actin filaments ratcheting *in vivo* against a load. Proceedings of the National Academy of Sciences, 111(50), 17845-17850.

Farhadifar, R., Rper, J. C., Aigouy, B., Eaton, S., and Jlicher, F. (2007). The influence of cell mechanics, cell-cell interactions, and proliferation on epithelial packing. Current Biology, 17(24), 2095-2104.

Fletcher, A. G., Osterfield, M., Baker, R. E., and Shvartsman, S. Y. (2014). Vertex models of epithelial morphogenesis. Biophysical journal, 106(11), 2291-2304.

Graner, F., and Glazier, J. A. (1992). Simulation of biological cell sorting using a two-dimensional extended Potts model. Physical review letters, 69(13), 2013.

Hannezo, E., Prost, J., and Joanny, J. F. (2014). Theory of epithelial sheet morphology in three dimensions. Proceedings of the National Academy of Sciences, 111(1), 27-32.

Heisenberg, C. P., and Bellache, Y. (2013). Forces in tissue morphogenesis and patterning. Cell, 153(5), 948-962.

Maitre, J. L., Berthoumieux, H., Krens, S. F. G., Salbreux, G., Julicher, F., Paluch, E., and Heisenberg, C. P. (2012). Adhesion functions in cell sorting by mechanically coupling the cortices of adhering cells. Science, 338(6104), 253-256.

Marcy, Y., Prost, J., Carlier, M. F., and Sykes, C. (2004). Forces generated during actin-based propulsion: a direct measurement by micromanipulation. Proceedings of the National academy of Sciences of the United States of America, 101(16), 5992-5997.

Mao, Y., Tournier, A. L., Hoppe, A., Kester, L., Thompson, B. J., and Tapon, N. (2013). Differential proliferation rates generate patterns of mechanical tension that orient tissue growth. The EMBO journal, 32(21), 2790-2803.

Marinari, E., Mehonic, A., Curran, S., Gale, J., Duke, T., and Baum, B. (2012). Live-cell delamination counterbalances epithelial growth to limit tissue overcrowding. Nature, 484(7395), 542-545.

Rauzi, M., Lenne, P. F., and Lecuit, T. (2010). Planar polarized actomyosin contractile flows control epithelial junction remodelling. Nature, 468(7327), 1110-1114.

Salbreux, G., Charras, G., and Paluch, E. (2012). Actin cortex mechanics and cellular morphogenesis. Trends in cell biology, 22(10), 536-545.

Sedzinski, J., Biro, M., Oswald, A., Tinevez, J. Y., Salbreux, G., and Paluch, E. (2011). Polar actomyosin contractility destabilizes the position of the cytokinetic furrow. Nature, 476(7361), 462-466.

Tsukita, S., Tsukita, S., Nagafuchi, A., and Yonemura, S. (1992). Molecular linkage between cadherins and actin filaments in cell-cell adherens junctions. Current opinion in cell biology, 4(5), 834-839.

Turlier, H., Audoly, B., Prost, J., and Joanny, J. F. (2014). Furrow constriction in animal cell cytokinesis. Biophysical journal, 106(1), 114-123.

Wu, S. K., Lagendijk, A. K., Hogan, B. M., Gomez, G. A., and Yap, A. S. (2015). Active contractility at E-cadherin junctions and its implications for cell extrusion in cancer. Cell Cycle, 14(3), 315-322.